J Paleolimnol
DOI 10.1007/s10933-013-9710-1

ORIGINAL PAPER

Paleoenvironmental implications of new OSL dates on the formation of the "Shell Bar" in the Qaidam Basin, northeastern Qinghai-Tibetan Plateau

ZhongPing Lai · Steffen Mischke · David Madsen

Received: 28 June 2012 / Accepted: 22 March 2013

Abstract A geological feature in the Qaidam Basin known as the "Shell Bar" contains millions of freshwater clam shells buried in situ. Since the 1980s, this feature in the now hyper-arid basin has been interpreted to be lake deposits that provide evidence for a warmer and more humid climate than present during late marine isotope stage 3 (MIS 3). Global climate during late MIS 3 and the last glacial maximum, however, was cold and dry, with much lower sea levels. We re-investigated the feature geomorphologically and sedimentologically, and employed optically stimulated luminescence (OSL) dating to verify the chronology of the sediments. We interpret the Shell Bar to be a remnant of a river channel formed by a stream that ran across an exposed lake bed during a regressive lake phase. Deflation of the surrounding older, fine-grained lacustrine deposits has left the fluvial channel sediments topographically inverted, indicating the erosive nature of the landscape. Luminescence ages place the formation of the Shell Bar in MIS 5 ($\sim$113–99 ka), much older than previous radiocarbon ages of <40 ka BP, but place the paleoclimatic inferences more in accord with other regional and global climate proxy records. We present a brief review of the age differences derived from ^{14}C and OSL dating of some critical sections that were thought to represent a warmer and more humid climate than present during late MIS 3. We attribute the differences to underestimation of ^{14}C ages. We suggest that ^{14}C ages older than $\sim$25 ka BP may require re-investigation, especially dates on samples from arid regions.

Keywords OSL dating · Depositional origin · Paleoenvironmental change · Late Pleistocene · Shell Bar · Qaidam Basin · Qinghai-Tibetan Plateau (QTP)

Z. Lai
CAS Key Laboratory of Salt Lake Resources and Chemistry, Qinghai Institute of Salt Lakes, Chinese Academy of Sciences, Xining 810008, China

Z. Lai (✉)
State Key Laboratory of Cryosphere Sciences, Cold and Arid Regions Environmental and Engineering Research Institute, Chinese Academy of Sciences, Lanzhou 730000, China
e-mail: zplai@isl.ac.cn; zplai@yahoo.com.cn

S. Mischke
Institute of Earth and Environmental Science, Universität Potsdam, 14476 Potsdam-Golm, Germany
e-mail: smischke@geo.uni-potsdam.de

S. Mischke
Institute of Geological Sciences, Freie Universität Berlin, 12249 Berlin, Germany

D. Madsen
Texas Archeological Research Laboratory, University of Texas, Austin, TX 78712, USA
e-mail: dmadsen@austin.rr.com

Published online: 02 April 2013

Introduction

The present climate of the Qinghai-Tibetan Plateau (QTP) is arid, and closed-basin saline lakes are widely distributed across its interior and adjacent margins. Li et al. (1991) revealed that paleoshorelines 60–160 m higher than present lake levels were common in the area, suggesting warmer and more humid climates when these high stands occurred. Radiocarbon (^{14}C) dating of some paleoshorelines suggested they formed 40–25 ka BP (Shi et al. 1999, 2001). This apparent high-stand period was termed the "Greatest Lake Period" (GLP) (Li and Zhu 2001). Since the GLP was first defined, supporting data have been recovered from the QTP and adjacent areas, including the Tengger, Badain Jaran, and Taklimakan deserts (Shi et al. 2001; Yang et al. 2004; Yu et al. 2007; Yang and Scuderi 2010). Reconstructions based on these data suggested temperatures were 2–4 °C higher than present on the QTP and that precipitation was 50–100 % higher than present during what was considered to be a "unique period of warm and humid climate in late MIS 3 in northwestern China" (Shi et al. 2001; Yu et al. 2007).

This reconstruction contrasts sharply with evidence that shows global climate during late MIS 3 (40–25 ka) was generally cold and dry (Imbrie et al. 1984; Prell and Kutzbach 1987). This lake-based GLP reconstruction is also markedly different from reconstructions of late MIS 3 climates in northwestern China based on other climate proxies, particularly those based on loess and pollen studies (Fang et al. 1999; Herzschuh 2006; Ning et al. 2009; Jiang et al. 2011; Long et al. 2012a). Moreover, recent shoreline studies of regional lake sequences using dating methods other than ^{14}C have also suggested that many lake high stands actually date to the MIS 5 (~129–71 ka) interglacial period (Zhu et al. 2004; Chen et al. 2008; Li et al. 2008; Madsen et al. 2008; Fan et al. 2010; Liu et al. 2010; Rhode et al. 2010; Long et al. 2012b; Zhang et al. 2012). A comparison of ^{14}C ages with the ages dated by other methods is presented in Fig. 1, which shows clear discrepancies between the dating approaches. The section locations are shown in Fig. 2.

To provide insight into these contrasting reconstructions, we initiated a study of the "Shell Bar," a geomorphic feature in the southeastern Qaidam Basin on the northeastern QTP (Fig. 3) that has often been used as evidence in support of the lake-based GLP reconstructions. Various ^{14}C dates have suggested the feature formed ~48–28 ka BP (Chen and Bowler 1986; Bowler et al. 1986; Chen et al. 1990) or ~40–18 ka BP (Zhang et al. 2007, 2008a). Initial geomorphic interpretations of the feature (Chen and Bowler 1985, 1986; Chen et al. 1990) suggested that the Shell Bar was part of a paleoshoreline formed during a high stand of a mega-lake that covered much of the Qaidam Basin. More recently, Zhang et al. (2007, 2008b) argued that it was a deep-water lacustrine deposit, whereas Lai (2012) proposed that it consists of fluvial sediments deposited within a river channel. In this study, we re-investigated the geomorphology and sedimentology of the Shell Bar, and employed optically stimulated luminescence (OSL) dating to determine the ages for the Shell Bar (Figs. 3 , 4).

Study area

The Qaidam Basin is located on the northeastern margin of the QTP (Fig. 3) and is a "canoe-shaped" inter-montane depression with a mean elevation of 2,800 m asl for the basin floor. It is surrounded by the Qilian, Kunlun, and Altun Mountains, which rise to more than 5,000 m asl. The basin has an area of about 120,000 km^2, and a catchment area of about 250,000 km^2 (Chen and Bowler 1986). The basin is dominated by the prevailing Westerlies, with mean annual temperatures of 2–4 °C (Chen and Bowler 1986). Maximum wind velocity occurs in the spring.

The modern Chaerhan salt lake lies in the east-central part of the Qaidam Basin, northeast of Golmud City, and was a depositional center of the basin during the Quaternary, with lacustrine deposits reaching ~3,000 m thickness (Liu et al. 1998). The Chaerhan salt lake playa occupies an area of 5,800 km^2, with an east–west length of 168 km, a south-north width of up to 40 km, and a height difference of only 2–5 m from end to end (Chen and Bowler 1985, 1986). The lake/playa has an elevation of 2,675 m asl at the lowest point in the depression (Chen and Bowler 1985). It is one of the driest places in the world, with annual precipitation of 24–40 mm and annual evaporation of 3,250 mm (Chen and Bowler 1985). Within the playa, water supplied by small rivers and groundwater forms nine saline lakes of different sizes. Salt deposits are dominant and account for ~70 % of a 50-m core collected by Chen and Bowler (1985). Higher-than-present lake levels have been documented in many

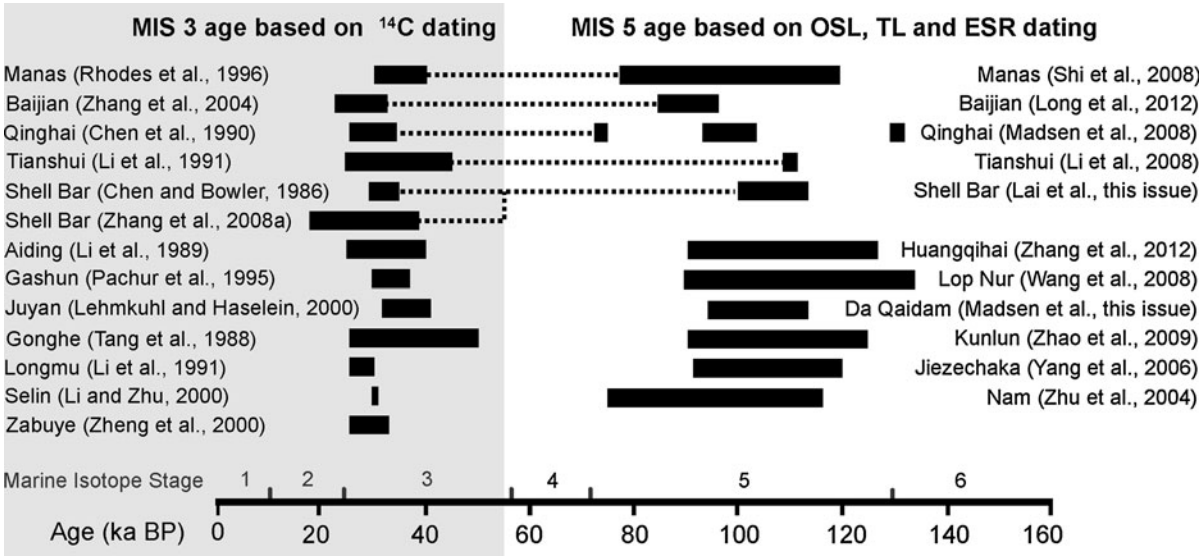

Fig. 1 Compilation of ^{14}C ages for high lake levels and ages by OSL, TL and ESR dating. The ^{14}C ages fall into late MIS 3 (*left column*), whereas the other ages are in MIS 5 (*right column*)

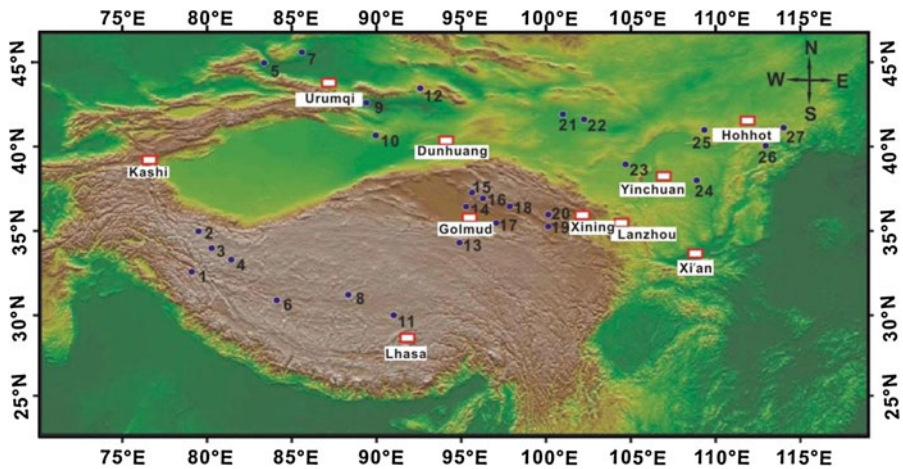

Fig. 2 Map showing the locations of lakes mentioned in the text. *1* Bangong, *2* Tianshui, *3* Longmu, *4* Jiezechaka, *5* Aibi, *6* Zabuye, *7* Manas, *8* Selin, *9* Aiding, *10* Lop Nur, *11* Nam Co, *12* Balikun, *13* Kunlun, *14* Chaerhan, *15* Da Qaidam, *16* Xiao Qaidam, *17* Shell Bar, *18* Gaihai, *19* Gonghe, *20* Qinghai, *21* Gashun, *22* Juyan, *23* Baijian, *24* Salawusu, *25* Hetao, *26* Daihai

places in the Qaidam Basin, reaching at least 36 m higher in the Balongmahai Lake sub-basin, at least 56 m higher in the Qidaoliang sub-basin, and 60–75 m in the Kunteyi sub-basin (with 7–8 shorelines) (Chen and Bowler 1985; Bowler et al. 1986).

The Shell Bar (Figs. 3, 4a) is located in the southeast portion of the Chaerhan playa, northwest of the town of Nuomuhong. It is the only known place in the Qaidam Basin that has shell preservation and is considered to be part of a Chaerhan paleolake shoreline (Chen and Bowler 1986; Chen et al. 1990). The Shell Bar has an east–west length of 2,130 m, a south-north width of up to 140 m, and stands of up to 2–3 m above the surrounding ground surface. Its surface varies from 2,698 to 2,702 m asl (2,700 m asl average). The top of the Shell Bar slopes from east to west, dropping ~2 m across its >2-km length (Zhang et al. 2007; Fig. 4). There are two springs on the western end of the Shell Bar (Fig. 4b, c). The larger spring mouth (Fig. 4c) has been artificially enlarged to

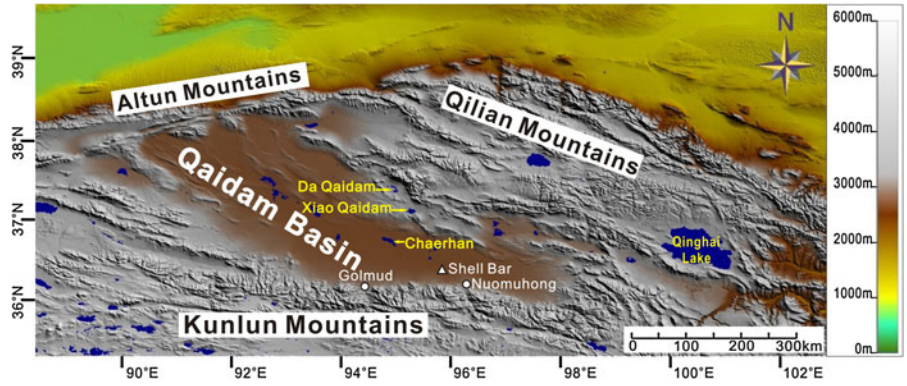

Fig. 3 The Qaidam Basin at the northern margin of the Tibetan Plateau, with the Shell Bar in its eastern part

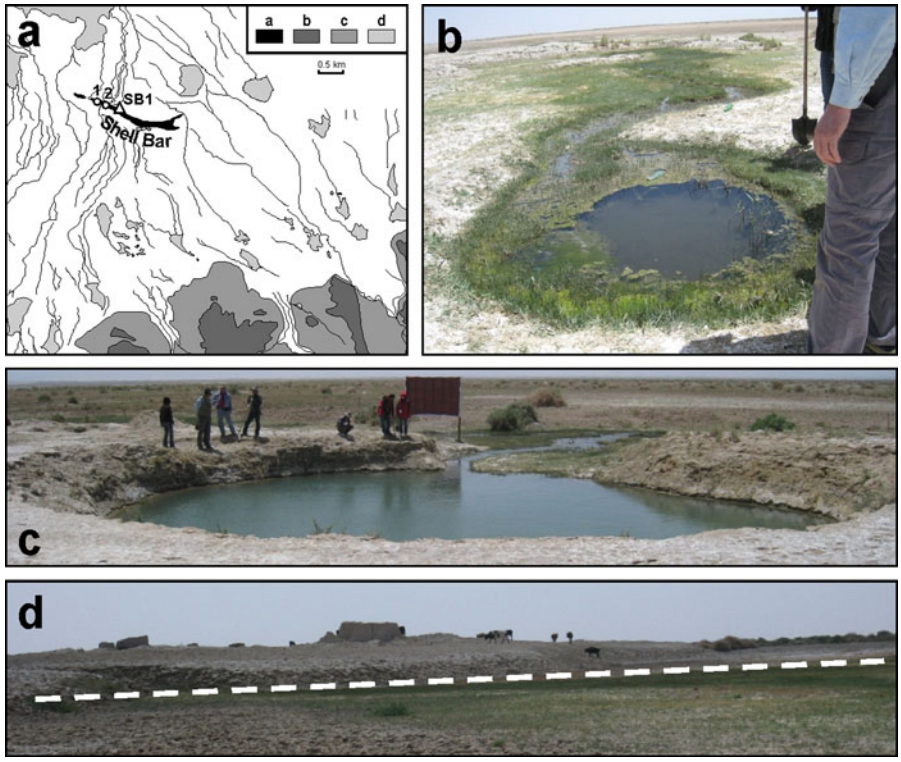

Fig. 4 **a** The Shell Bar (*black*) and its vicinity (modified from Mischke et al. 2013). The *empty triangle* in the middle of the Shell Bar is the SB1 section, and the *two open circles* in the Shell Bar represent the locations of two spring mouths ("*1*" is the large spring and "2" is the small spring). Legends: *a* extent of the Shell Bar; *b* exposed fluvial and lacustrine sediments in the south of the Shell Bar; *c* assumed extent of fluvial and lacustrine sediments; *d* modern salt flats (playas). **b** View of the smaller unaltered spring, looking north). **c** View of the larger spring, looking south, that has been enlarged to attract tourists. **d** View of the Shell Bar, looking north at ground level. The *white*, *dashed line* marks the foot of the Shell Bar. Ruins of abandoned houses and a few cows on the top of the Shell Bar provide a scale for the photo

attract tourists, but the smaller one remains undisturbed (Fig. 4b). The Shell Bar is composed primarily of millions of densely packed, articulated shells, buried in situ (Fig. 5), and most of the shells come from freshwater taxa (Chen and Bowler 1986; Mischke et al. 2013).

Materials and methods

Section SB1 (36.5140°N, 96.2021°E, 2696 m asl) is located in the central part of the Shell Bar (Fig. 4a) and can be divided into four units (Fig. 5a). From the bottom to the top, unit 4, the base of which was not

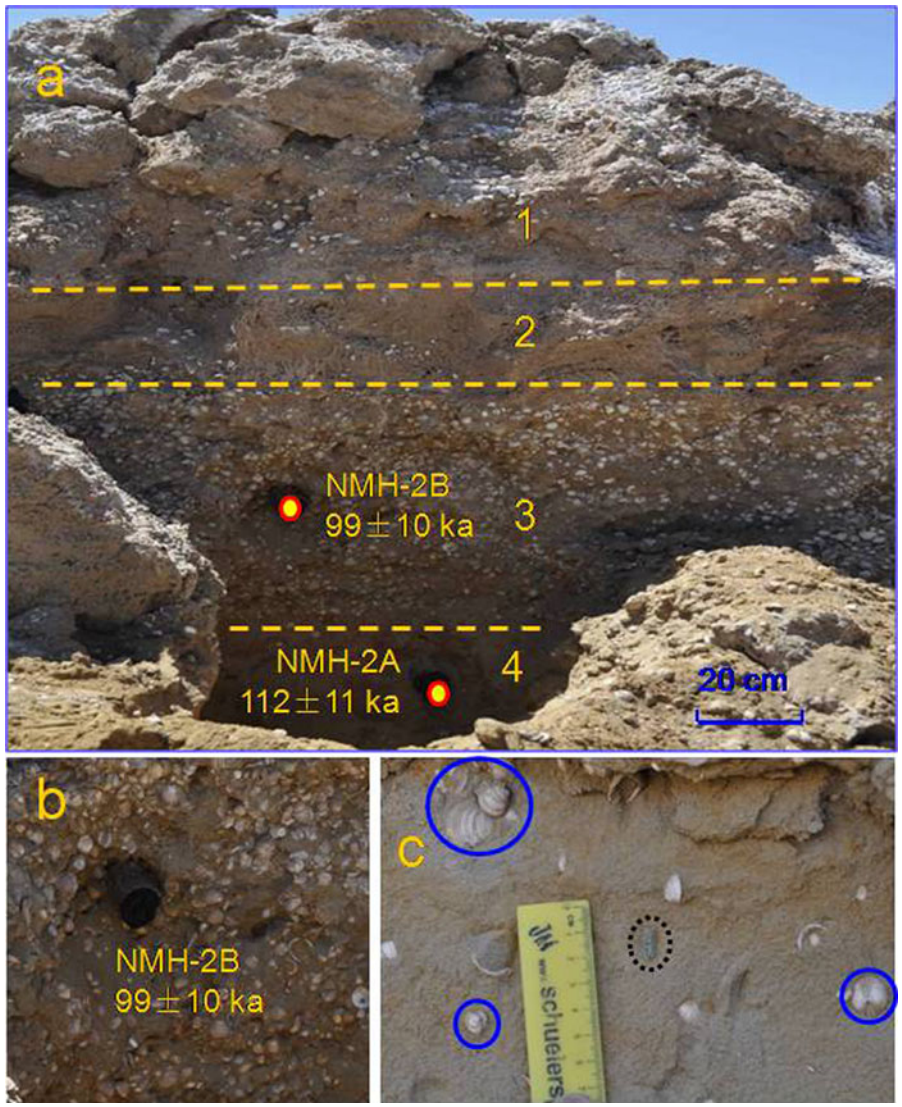

Fig. 5 **a** View of the SB1 section, together with OSL ages. The section can be divided into four units (*1*, *2*, *3*, and *4*). See text for a detailed description. The *white dots* are all shells. For scale, unit 2 is ∼20 cm thick. **b** Close-up of unit 3 and location of sample NMH-2B. The diameter of the sample tube is ∼4.2 cm. **c** Close-up of unit 4, showing scattered, articulated shells (in *blue circles*) and gravels (in *black dotted-circle*). (Color figure online)

uncovered, is composed of yellowish-brown silty fine sand, containing some scattered gravels up to 2 cm in diameter (Fig. 5c). OSL sample NMH-2A was collected from this unit. Unit 3, with a thickness of ∼48 cm, is composed of a salt-cemented silty fine sand matrix containing densely packed, mostly articulated shells. OSL sample NMH-2B was collected from the middle of the unit. Unit 2, with a thickness of ∼20 cm, covers the whole Shell Bar and has a porous salt crust overlying densely packed broken and articulated shells, mostly within a matrix of fine sand. Uppermost Unit 1 is disturbed material with a thickness of about 1 m. It also contains scattered articulated shells (Fig. 5c) with carapaces larger than those in Unit 3. Bulk samples from the SB section, a few m from the SB1 section, were collected for sedimentological (grain size and total organic carbon), paleoecological (bivalve, ostracods), and taphonomical (size measurements, records of articulated shells) analyses. These results are reported by Mischke et al. (2013).

OSL sample preparation and measurement

OSL samples were collected by hammering steel tubes, ~20 cm long and ~4-cm in diameter, into freshly cleaned profiles. The tubes were then covered with aluminum foil and sealed with opaque tape. Bulk samples for water content and radioactive element measurements were also collected for each OSL sample location and sealed immediately to ensure that the sediment retained its original water content.

In the laboratory, under red light conditions, about 3–4 cm of material from each end of the tube was removed, and the middle portion was used to extract quartz for equivalent dose (D_e) determination. Samples were treated first with 10 % HCl and 30 % H_2O_2 to remove carbonate and organic matter, respectively. The 38–63-μm fraction was used for OSL dating because it was the dominant grain size in the samples (Mischke et al. 2013). The fraction was extracted by sieving, and then etched with 35 % H_2SiF_6 for about 2 weeks to remove feldspars (Lai et al. 2007a; Lai 2010). The resulting quartz grains were washed with 10 % HCl to remove fluoride precipitates. The purity of quartz grains was checked by IR (830 nm) stimulation (Duller 2003). Any samples with obvious infrared stimulated luminescence (IRSL) signals were retreated with H_2SiF_6 to avoid D_e underestimation (Lai and Brückner 2008). The quartz grains were then mounted as a mono-layer on the center (diameter ~0.5 cm) of stainless steel discs (diameter 1 cm), using silicone oil.

OSL measurements were made using an automated Risø TL/OSL-DA-20 reader equipped with blue diodes ($\lambda = 470 \pm 20$ nm) and IR laser diodes ($\lambda = 830$ nm). Ninety percent diode power was used. The luminescence stimulation used blue LEDs at 130 °C for 40 s, and the OSL signal was detected by a 9235QA photo-multiplier tube, through a 7.5-mm-thick U-340 filter (detection window 275–390 nm). Irradiations were carried out using a $^{90}Sr/^{90}Y$ beta source built into the Risø reader.

The chosen preheat temperature was 260 °C for 10 s for natural and regenerative doses, and the cut-heat temperature was 220 °C for 10 s for test doses. These conditions were determined after a preheat plateau test and a dose recovery test (Murray and Wintle 2003). Signals of the first 0.64 s stimulation were integrated for growth curve construction after background subtraction (last 5 s). Concentrations of U, Th, and K were measured by neutron activation analysis. The cosmic-ray dose rate was estimated for each sample as a function of depth, altitude and geomagnetic latitude (Prescott and Hutton 1994). For the 38–63-μm grains, the alpha efficiency value was taken as 0.035 ± 0.003 (Lai et al. 2008). Finally, elemental concentrations were converted into annual dose rates according to Aitken (1998).

Equivalent dose (D_e) determination

In the current study, the SAR protocol (Murray and Wintle 2000) and the standard growth curve (SGC) method (Roberts and Duller 2004; Lai 2006; Lai et al. 2007b) were employed for D_e determination. For each sample, six aliquots were measured using the SAR protocol to obtain six D_es and six growth curves. These six growth curves were then averaged to construct a SGC for each individual sample. Then, the values of standardized natural signal (L_N/T_N) were measured for more aliquots, using the same measuring conditions used in the SAR protocol. The value of L_N/T_N in each aliquot was then matched in the SGC to obtain a D_e. D_e results determined by the SGC are in agreement with those by the SAR protocol (Table 1), suggesting that

Table 1 Quartz OSL dating results for the Shell Bar

Sample ID	Depth (m)	K (%)	Th (ppm)	U (ppm)	Dose rate (Gy/ka)	No. of aliquots	SAR D_e (Gy)	SGC D_e (Gy)	Final D_e (Gy)	OSL Age (ka)
NMH-2B	1.44	1.70 ± 0.09	5.47 ± 0.19	1.12 ± 0.19	2.52 ± 0.23	6[a] + 20[b]	249 ± 15	248 ± 8	248 ± 7	99 ± 10
NMH-2A	1.78	1.65 ± 0.06	6.09 ± 0.19	1.41 ± 0.12	2.58 ± 0.22	6[a] + 16[b]	293 ± 12	289 ± 14	290 ± 10	113 ± 10

For all samples, quartz grain size of 38–63 μm is used for D_e determination. Water content for both samples was taken as 10 ± 7 %. In a hyper-arid climate it is a little bit higher, but the site is the depocenter of the basin and the sediment is of aquatic nature. The large error is to accommodate the uncertainty of the water content during the burial

[a] Number of aliquots by SAR, and [b] number of aliquots by SGC

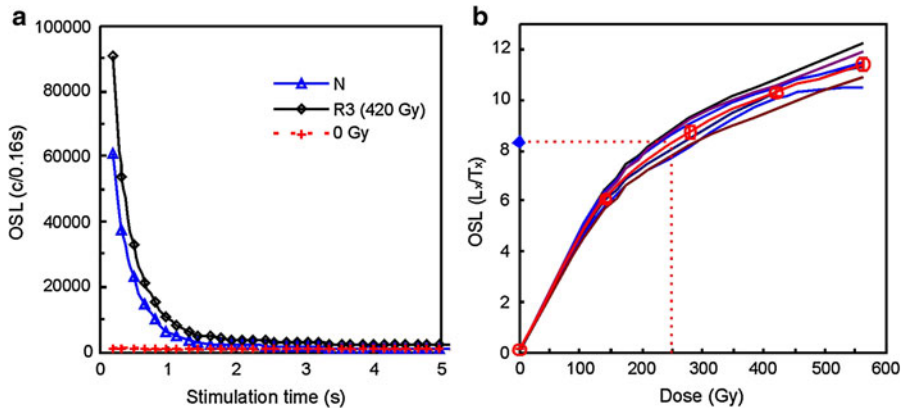

Fig. 6 Luminescence characteristics of sample NMH-2B. **a** The quartz OSL shine-down curves for the natural and regeneration doses of 420 Gy and 0 Gy, respectively. The curve of 0 Gy shows that recuperation is negligible. **b** Growth curves for six aliquots and the average growth curve (*red line with empty red circle*) of the six growth curves. The growth curve does not saturate up to 600 Gy, and could be fitted well using an exponential plus linear function. (Color figure online)

the SGC could be used for D_e determination for samples from the Qaidam Basin. The final D_e of each sample is the mean of all SAR D_es and SGC D_es.

Results

Figure 6a shows typical OSL decay curves of sample NMH-2B. OSL signals decrease very quickly during the first second of stimulation, indicating that the OSL signal is dominated by the fast component. Recuperation was calculated by comparing the sensitivity-corrected OSL signal of 0 Gy to the sensitivity-corrected natural signal. The recuperation was <1 % for all samples. The 'recycling ratio' was introduced to check for sensitivity change correction (Murray and Wintle 2000). For all aliquots, the recycling ratios fall into the acceptance range of 0.9–1.1. Figure 6b shows the growth curves of six individual aliquots, as well as the SGC for sample NMH-2B. The growth curve does not saturate up to 600 Gy, and can be well fitted using the exponential plus linear function. OSL dates are listed in Table 1 and shown in Fig. 5. The ages for the two OSL samples are 99 ± 10 ka (sample NMH-2B) and 113 ± 10 ka (sample NMH-2A), and fall within MIS 5.

Discussion

Three conventional radiocarbon dates on shells were reported (Chen and Bowler 1986; Huang and Cai 1987): 28.63 ± 0.67 ^{14}C ka BP at a depth of 0.05–0.25 m, 35.10 ± 0.90 ^{14}C ka BP at a depth of 1.1–1.2 m, and 38.60 ± 0.68 ^{14}C ka BP at a depth of 1.7–1.8 m, the base of the shell deposit. Using these data, Chen et al. (1990) suggested that the climate was humid and warm, with high lake levels in the Qaidam Basin during the period of 38–28 ^{14}C ka BP, that is, during a supposedly humid late MIS 3 period. Pollen data from Chaerhan lake cores Chen and Bowler (1986) and archaeological evidence from Xiao Qaidam Lake (Huang et al. 1987) were also thought to support a warm and humid MIS 3 interpretation.

Without knowledge of the details of the radiocarbon dating, it is difficult to evaluate the reliability of the ^{14}C ages reported by Chen and Bowler (1986) and Huang and Cai (1987). Bowler et al. (1986) conducted detailed conventional ^{14}C dating on carbonates from the Qaidam Basin, including shorelines in Kunteyi and Xiao Qaidam, and cores from Chaerhan. Carbonates provided ages of stratigraphic irregularity, imposing limits on dating reliability. Sample ANU 2975 from the surface of the Chaerhan playa gave an age of 23.90 ± 0.53 ^{14}C ka BP, in contrast to the result of Huang et al. (1981), which, on an age-depth curve, displayed an extrapolated age near zero age at the surface.

Zhang et al. (2007, 2008a) re-visited the Shell Bar and collected about 90 samples for detailed analyses of chronology and climate proxies (geochemistry, fossils, mineralogy, grain size). They used both ^{14}C and U-series dating methods, and also compared results from different laboratories in China, Germany and

USA. They also tried to date different materials for comparison (total organic and inorganic carbon, shells, salt crystals) and provided details of dating procedures. They obtained more than 40 ^{14}C and U-series ages and found that the ^{14}C ages of shells were 15–18 ^{14}C ka older than ages for organic matter collected from the same depth. The authors suggested that among these ages, only four AMS ^{14}C ages on organic matter, run at Kiel University, Germany, were reliable: 22.11 ± 0.19 ^{14}C ka BP at 0.53 m, 28.98 + 0.51/−0.48 ^{14}C ka BP at 1.245 m, 29.42 + 0.63/−0.59 ^{14}C ka BP at 1.39 m, and 30.51 + 0.65/−0.60 ^{14}C ka BP at 1.52 m. Using interpolation and extrapolation, they established a depth-age relationship for the whole section and calculated an age of 17.5 ^{14}C ka BP for the surface (0 m) and an age of 39.7 ^{14}C ka BP for the base of the section (depth 2.55 m), where the sediment was regarded to represent the beginning of a high lake-level period. They concluded that the Shell Bar deposition was continuous and represents a period of high lake level, with an age range of 39.7–17.5 ^{14}C ka BP. This chronology contrasts with that by Huang and Cai (1987), who proposed an age range of 38–28 ^{14}C ka BP. Zhang et al. (2007) also reported U-series dating results from the University of Minnesota, USA for three salt crystal samples collected from the top of the section, with ages of 158.4 ± 18 ka, 158 ± 15 ka, and 119.3 ± 16 ka. Because these ages are so much older than the ^{14}C dates, they were considered unreliable and rejected by the authors. Huang et al. (1990) also collected two surface halite crystal samples from the Chaerhan playa, at a location ~90 km further NW, which provided U-series ages of 16 ± 1.3 ka and 12 ± 1.1 ka, but they present no dating details. They concluded that the Chaerhan region has been a playa since about 16 ka.

Origin of the Shell Bar

Different views have been proposed to account for deposition of the Shell Bar. Based on geomorphology and shell analysis, Chen and Bowler (1985, 1986) and Chen et al. (1990) hypothesized the Shell Bar formed along the shoreline of a fresh to slightly saline lake. Subsequently, using field observations of its sedimentary structure combined with the ostracod assemblage, Zhang et al. (2007) suggested that the Shell Bar depositional sequence was continuous and that it formed under water. Zhang et al. (2008b) inferred a deep and stagnant water body because of the mass occurrence of *Corbicula* shells. They agreed with the earlier research that suggested there was a large freshwater lake at that time that existed as a result of a warmer and more humid climate than present.

In contrast, using field geomorphological and sedimentological observations, Lai (2012) proposed that the Shell Bar is a fluvial deposit formed in a now topographically inverted river channel. This view is in agreement with Mischke et al. (2013) who argue that the largely unbroken nature and dense concentration of the *Corbicula* shells likely rules out the possibility they were deposited in a beach/shoreline sediment that was subject to extensive wave action. Furthermore, if the Shell Bar is a remnant of a deeper lake, then a larger, three-dimensional extension of sediments would be present in other areas of that lake. Because the Shell Bar is the only geological structure of its kind within the Qaidam Basin, that appears not to be the case.

The form of the Shell Bar itself is suggestive of river deposition. The sinuous nature of the feature, as opposed to a flat irregular shape that would result if it were a remnant of a deep-water deposit, suggests a riverine environment. Moreover, presence of perennial springs at the toe of the feature indicates groundwater flows along its length. The sand matrix that holds the *Corbicula* shells is far more permeable than the dense, deep-water lacustrine mud in which the feature sits, and the presence of the springs suggests flow along the Shell Bar. In addition, the *Corbicula* species represented in the Shell Bar, *C. largillierti* and *C. fluminea*, generally thrive in the flowing waters of large streams and estuaries, which represent high-energy settings, suggesting deposition within a stream channel rather than in deep lake waters (Mischke et al. 2013).

We conclude that the Shell Bar consists of river-channel sediments and speculate that it was formed when a river or stream flowed across, and incised a channel into, the lake sediments, which were left behind when a large lake in the Qaidam Basin regressed to very low levels. A population of *Corbicula* prospered in an area of slower stream flow or perhaps in a cut-off distributary. As the water table dropped and the lake sediments were exposed to wind erosion, the shells themselves formed a more resistant sediment package, leaving them topographically inverted as the surrounding sediments were deflated. The thin layer (~10–20 cm) of salt crust on top of the

Shell Bar helped protect it from the deflation. Similar situations occur in both the Gaxun Nur Basin of western China (Hartmann et al. 2011) and the Bonneville Basin of western North America (Oviatt et al. 2003), where distributary streams of paleo-deltas formed after the regression of large pluvial lakes and now lie topographically inverted. A test of this hypothesis would involve following the Shell Bar channel up or downstream using ground-penetrating radar or simply by digging.

Paleoenvironmental implications of the OSL ages

We present here the first OSL dates for the Shell Bar. The OSL ages (Table 1; Fig. 5) fall into MIS 5, suggesting that fluvial sediments accumulated during the last interglacial period. As we have noted above, since the 1980s the Shell Bar has been thought to date to late MIS 3 or even early MIS 2. Li and Zhu (2001) summarized and termed this period the "GLP," and according to their calculations, the total area of the studied lakes during the GLP was 14.9 times larger than that of the present. Follow-up studies have also referred to the interval as the "pan-lake stage" (Zheng et al. 2000) and a "unique period of warm and humid climate" (Shi et al. 2001). The Shell Bar, in a now hyper-arid, inland basin, has been a key site supporting these views.

Simulations have suggested the climate pattern in northern China at 35 ka BP was warm–wet (Yu et al. 2007), seemingly in agreement with the GLP interpretation. Further, an investigation of the Guliya ice core in the QTP by Thompson et al. (1997), showed that interstadial MIS 3 was marked by increases in $\delta^{18}O$ values similar to those of the Holocene and Eemian (124 ka ago, MIS 5e). As a result, the climate pattern in northern China during 40–25 ka has been thought to be quite different from the global pattern (Shi et al. 1999). Growing chronological evidence, especially other than ^{14}C dates, suggests that this "unique" climate pattern in late MIS 3 in northwest China may simply be a consequence of age underestimations related to ^{14}C dating, and that the geological evidence for a markedly warm and humid period in truth dates to MIS 5 rather than late MIS 3. In a recent review of research on Qinghai Lake in the northeastern QTP, Colman et al. (2007) concluded that "lacustrine carbonate $\delta^{18}O$ records reveal no climatic anomaly during MIS 3, so that high terraces interpreted as evidence for extremely high lake levels during MIS3 remain an enigma." Based on OSL dating, Madsen et al. (2008) showed that the highest levels of Qinghai Lake occurred in MIS 5. Other dating work, using techniques other than ^{14}C, also showed that the highest lake levels in both the Qaidam Basin (Mischke et al. 2010) and Nam Co Lake in the interior of the QTP (Zhu et al. 2004) existed in MIS 5 or earlier. Pollen data from the Lanzhou area of the western Chinese Loess Plateau showed that the later MIS 3 period was drier than present (Jiang et al. 2011), as do estimates of effective precipitation derived from loess sequences (Fang et al. 1999; Ning et al. 2009) and from a variety of climate proxy records.

Since 2008, one of us (ZPL) has organized a research program to systematically re-visit and re-date (using primarily OSL) many of the representative sites/sections used to support the interpretation of a warm and humid late MIS 3. The new OSL results, in all cases, have shown that the sediments representing high lake levels, previously dated by ^{14}C to late MIS 3, actually formed in MIS 5. Besides the Shell Bar discussed in this paper and in Mischke et al. (2013), these sites include Qinghai Lake (Liu et al. 2010; Liu and Lai 2010; Lai 2012), Gahai Lake in the Qaidam Basin (Fan et al. 2010), Xiao Qaidam Lake and Da Qaidam Lake in the Qaidam Basin (Sun et al. 2010; Madsen et al. 2013), Baijian Paleolake in the Tengger Desert (Long et al. 2012b), Huangqihai Lake in Inner Mongolia (Zhang et al. 2012), and the coastal Bohai Sea to the east of Beijing, where sea transgression rather than high lake level was investigated (Yi et al. 2013). Also, aeolian deposits in both Qinghai Lake region (Liu et al. 2012) and the Qaidam Basin (Yu and Lai 2012; Yu et al. in press) were formed since deglaciation. The research group has also shown that in the Qinwangchuan Basin in the Lanzhou area of the western Chinese Loess Plateau, paleodunes intercalated in thick loess occurred ca. 35–25 ka, implying a period of increased aridity with dune formation (Long et al. 2012b). This is in contrast to previously retrieved, lake archives from nearby deserts (e.g., the Tengger and Badain Jaran deserts), indicating a humid episode during MIS 3. They have also shown that no lake highstands were observed for MIS 3 and MIS 2 in the endorheic basin of Huangqihai Lake, in Inner Mongolia (north China), and that loess deposits formed ~50–20 ka on top of ~90–ka-old lacustrine sediments, indicating a drier climate in MIS 3 than in

MIS 5 (Zhang et al. 2012). The group also found that glacial advances during MIS 3 at Yingpu Valley of the Hengduan Mountains, in the eastern QTP, apparently responded to cold stages or cold events rather than to episodes of enhanced summer monsoon and moisture, and, as a result, glaciers in the monsoonal Hengduan Mountains were mainly controlled by changes in temperature (Ou et al. 2012). This conclusion does not support a warm and humid MIS 3 in the QTP because a warmer than present climate in MIS 3 would not allow glacial development to such an extent.

The new MIS 5 OSL ages presented here put the paleoclimatic interpretation of the sediments in accord with published climatic proxy data for the Shell Bar (Chen and Bowler 1986; Zhang et al. 2007, 2008a, b, c; Mischke et al. 2013), suggesting it formed under a warm climate and in fresh or slightly brackish water. In particular, Mischke et al. (2013) argued that the mass occurrence of *Corbicula* in the Qaidam Basin indicates that climate conditions were probably slightly warmer than today, and tentatively proposed that summer temperatures $\sim$1 °C higher than at present occurred during the time of the Shell Bar formation.

Further confirmation of this MIS 5 age may be useful, but regardless of its age, it is clear the Shell Bar post-dates any Qaidam Basin mega-lake. It was formed by an active stream or a river that flowed into the Chaerhan playa from the eastern Kunlun Mountains after a lake regressed from the basin floor. Exactly when that lake regressed, and how much earlier than the formation of the Shell Bar, is unclear. The river incised a channel into the lacustrine muds of that former lake, and the accumulation of *Corbicula* shells in the Shell Bar locality and the thin salt crust layer on top provided resistance to the erosional forces that have deflated the surrounding lake sediments, leaving it in topographical relief. At present, the paleochannel rises up to 2–3 m above the playa, and because the Chaerhan playa was the depositional center of the inland Qaidam Basin during the Quaternary, this implies that the area has experienced considerable deflation and erosion since MIS 5. Discussion of this erosion in the Qaidam Basin may shed light on past atmospheric circulation patterns, dust transport and deposition, and the source of loess in the Chinese Loess Plateau. This, however, is beyond the scope of this paper and will be discussed elsewhere.

Possible reasons for underestimation of radiocarbon ages

As noted above, OSL ages of the highstands in many lakes in northwestern China fall into MIS 5, whereas most ^{14}C ages for the same shorelines fall into late MIS 3 ($\sim$40–30 ka BP) or even younger periods. These differences suggest the ^{14}C ages are severely underestimated, regardless of whether ^{14}C ages were determined by AMS or the conventional method, or whether the dated carbon was organic or inorganic.

Shells of freshwater bivalves are often considered to be one of the most reliable materials for ^{14}C dating (Rick et al. 2005). Sample contamination during burial, however, may lead to severe age underestimation. During pretreatment of bivalve shells for ^{14}C dating, it is essential to determine if diagenetic alteration of original shell aragonite has resulted in replacement by meteoric calcite. For charcoal and eggshell samples, chemical pretreatments can remove contaminants (Bird et al. 2003). Usually, diagenetic alteration of freshwater shells produces calcite and not aragonite (Zhou et al. 1999). According to Webb et al. (2007), aragonite cement rather than calcite can form in an environment where the Mg/Ca ratio of local groundwater is unusually high. As a result, diagenetically affected freshwater bivalve shells that do not contain calcite may be erroneously interpreted as unaltered, even though they contain diagenetic ^{14}C that may not be detected by common vetting techniques. These shells will cause underestimation of ages by radiocarbon dating. As an example, Webb et al. (2007) demonstrated that underestimated ^{14}C ages for shell samples from Darling Downs, Australia were caused by diagenetic alteration that introduced young aragonite into the samples. They showed that paired samples, with and without contamination by younger aragonite, returned ages of 24.1 $\pm$ 0.2 and 33.9 $\pm$ 0.6 ka, respectively. In an arid setting characterized by ephemeral saline lakes with high Mg/Ca ratios, such as the Shell Bar environment, shells may suffer from this diagenetic alteration.

Besides contamination from burial, which may go undetected as discussed above, contamination can also result from incomplete removal of atmospheric C species that are introduced during laboratory processing, or by sample "cross talk," as suggested by Pigati et al. (2007). Equally important is that the impact of contamination increases with sample age. For

example, a 2 % contamination with modern carbon of a 15-ka-old sample may lead to only a minor age underestimation, whereas the same contamination for a 60-ka-old sample would yield an age estimate of only ~30 ka (Pigati et al. 2007).

Radiocarbon-age underestimation for sediment samples has caused confusing chronologies in Late Quaternary paleoenvironmental studies in many places throughout the world, but recent OSL dating has successfully corrected these underestimations in many cases. For e.g., Simms et al. (2009) found that the age of "MIS 3 deposition" of shallow-marine sediment was actually OSL-constrained to MIS 5 (~90 ka) in the northwestern Gulf of Mexico. Briant and Bateman (2009) compared a set of paired OSL and AMS ages within Devensian fluvial sediments in lowland Britain, and showed that radiocarbon dating yielded MIS 3 ages of 30–40 ka BP, whereas OSL dating yielded last inter-glacial ages of 69–110 ka. They argued that radiocarbon-dated materials were contaminated by small fractions of modern carbon. Based upon the comparison between U-series dates and radiocarbon dates of borehole sediments, Yim et al. (1990) concluded that the transgression 2 deposited in Hong Kong formed in MIS 5, not in MIS 3, as previously suggested by ^{14}C. As a result, previous ^{14}C ages older than 25 ka BP may require re-investigation, especially for samples from arid regions.

Conclusions

Since the 1980s, the Shell Bar has been treated as one of the key sites supporting an inference for a warmer and more humid climate than present in the QTP and adjacent arid China during late MIS 3. Our new OSL ages suggest it was formed in MIS 5, instead of late MIS 3. This new chronology is in agreement with published regional climate proxy data and with the global climate pattern. We propose that the Shell Bar is a river channel deposit that is not related to lake deposition as previously thought, and that it post-dates any Qaidam Basin mega-lake. Deflation of fine-grained sediments surrounding the Shell Bar caused the topographically inverted relief that is seen today, indicating that the Quaternary deposition center of the Qaidam Basin experienced significant erosion since the formation of the Shell Bar.

Acknowledgments We thank two anonymous reviewers and the editor Mark Brenner for constructive comments. This work was supported by China NSF (41290252, 41121001), a SKLCS grant (SKLCS-ZZ-2012-01-04), and the One-Hundred Talent Project of CAS granted to ZPL (A0961).

References

Aitken MJ (1998) An introduction to optical dating: the dating of Quaternary sediments by the use of photon-stimulated luminescence. Oxford University Press, Oxford

Bird MI, Turney CSM, Fifield LK, Smith MA, Miller GH, Roberts RG, Magee JW (2003) Radiocarbon dating of organic- and carbonate carbon in *Genyornis* and *Dromaius* eggshell using stepped combustion and stepped acidification. Quat Sci Rev 22:1805–1812

Bowler JM, Huang Q, Chen KZ, Head MJ, Yuan BY (1986) Radiocarbon dating of playa-lake hydrological changes: examples from northwestern China and central Australia. Palaeogeogr Palaeoclimatol Palaeoecol 54:241–260

Briant RM, Bateman MD (2009) Luminescence dating indicates radiocarbon age underestimation in Late Pleistocene fluvial deposits from eastern England. J Quat Sci 24:916–927

Chen KZ, Bowler JM (1985) Preliminary study of sedimentary characteristics and evolution of palaeoclimate of Qarhan salt lake in Qaidam Basin. Sci Sin B 28:1218–1232

Chen K, Bowler JM (1986) Late Pleistocene evolution of salt lakes in the Qaidam Basin, Qinghai Province, China. Palaeogeogr Palaeoclimatol Palaeoecol 54:87–104

Chen K, Bowler JM, Kelts K (1990) Palaeoclimatic evolution within the Qinghai-Xizang (Tibet) Plateau in the last 40000 years. Quat Sci 3:21–31 (in Chinese with English abstract)

Chen FH, Fan Y, Chun X, Madsen DB, Oviatt CG, Zhai H, Yang LP, Sun Y (2008) Preliminary research on megalake Jilantai-Hetao in the arid areas of China during the Late Quaternary. Chin Sci Bull 53:1725–1739

Colman SM, Yu SY, An Z, Shen J, Henderson ACG (2007) Late Cenozoic climate changes in China's western interior: a review of research on Lake Qinghai and comparison with other records. Quat Sci Rev 26:2281–2300

Duller GAT (2003) Distinguishing quartz and feldspar in single grain luminescence measurements. Radiat Meas 37:161–165

Fan QS, Lai ZP, Long H, Sun YJ, Liu XJ (2010) OSL chronology for lacustrine sediments recording high stands of Gahai Lake in Qaidam Basin, Northeastern Qinghai–Tibetan Plateau. Quat Geochron 5:223–227

Fang X, Ono Y, Fukusawa H, Pan B, Li J, Guan D, Oi K, Tsukamoto S, Torii M, Mishima T (1999) Asian summer monsoon instability during the past 60,000 years: magnetic susceptibility and pedogenic evidence from the western Chinese Loess Plateau. Earth Planet Sci Lett 168:219–232

Hartmann K, Wünnemann B, Hölz S, Kraetschell A, Zhang H (2011) Neotectonic constraints on the Gaxun Nur inland basin in north-central China, derived from remote sensing, geomorphology and geophysical analyses. Geol Soc London Spec Pub 353:221–233

Herzschuh U (2006) Palaeo-moisture evolution in monsoonal Central Asia during the last 50,000 years. Quat Sci Rev 25:163–178

Huang Q, Cai BQ (1987) Geochronological study on the sediments in Qarhan Lake. Proceedings of the Sino-Australian Quaternary meeting, 106–114 (in Chinese with English abstract)

Huang Q, Cai BQ, Yu JQ (1981) The ^{14}C age and cycle of sedimentation of some saline lakes on the Qinghai-Xizang Plateau. Chin Sci Bull 26:66–70

Huang WW, Chen KZ, Yuan BY (1987) Paleolithics of Xiao Qaidam Lake in Qinghai Province in China. Proceedings of the Sino-Australian Quaternary meeting, pp 168–172 (in Chinese)

Huang Q, Meng ZQ, Liu HL (1990) A preliminary study on the climatic change pattern of the Chaerhan Lake in the Qaidam Basin. Sci China 6:652–663 (in Chinese)

Imbrie J, Hays JD, Martinson DC, McIntyre A, Mix AC, Morley JJ, Pisias NG, Prell WL, Shackleton NJ (1984) The orbital theory of Pleistocene climate: support from the revised chronology of the marine $\delta^{18}O$ record. In: Berger AL, Imbrie J, Hays J, Kukla G, Saltzman B (eds) Milankovich and Climate Part I. Reidel, Dordrecht, pp 269–305

Jiang H, Mao X, Xu H, Thompson J, Wang P, Ma X (2011) Last glacial pollen record from Lanzhou (northwestern China) and possible forcing mechanisms for the MIS 3 climate change in Middle to East Asia. Quat Sci Rev 30:769–781

Lai ZP (2006) Testing the use of an OSL standardized growth curve (SGC) for D_e determination on quartz from the Chinese Loess Plateau. Radiat Meas 41:9–16

Lai ZP (2010) Chronology and the upper dating limit for loess samples from Luochuan section in Chinese Loess Plateau using quartz OSL SAR protocol. J Asian Earth Sci 37: 176–185

Lai ZP (2012) Was late marine isotope stage (MIS) 3 warm and humid in nowadays arid northwestern China? Quat Int 279–280:261

Lai ZP, Brückner H (2008) Effects of feldspar contamination on equivalent dose and the shape of growth curve for OSL of silt-sized quartz extracted from Chinese loess. Geochronometria 30:49–53

Lai ZP, Brückner H, Zöller L, Fülling A (2007a) Existence of a common growth curve for silt-sized quartz OSL of loess from different continents. Radiat Meas 42:1432–1440

Lai ZP, Wintle AG, Thomas DSG (2007b) Rates of dust deposition between 50 ka and 20 ka revealed by OSL dating at Yuanbao on the Chinese Loess Plateau. Palaeogeogr Palaeoclimatol Palaeoecol 248:431–439

Lai ZP, Zöller L, Fuchs M, Brückner H (2008) Alpha efficiency determination for OSL of quartz extracted from Chinese loess. Radiat Meas 43:767–770

Lehmkuhl F, Haselein F (2000) Quaternary paleoenvironmental change on the Tibetan Plateau and adjacent areas (Western China and Western Mongolia). Quat Int 65–66:121–145

Li SJ, Li SD (1991) The study on two cores from Tianshuihai in the west Kunlun and its implications. J Glaciol Geocryol 13:187–188 (in Chinese)

Li BY, Zhu LP (2001) "Greatest lake period" and its palaeoenvironment on the Tibetan Plateau. J Geograph Sci 11: 34–42

Li BX, Cai BQ, Liang QS (1989) The sedimentological characteristics of Aiding lake in the Turpan Basin in west China. Chin Sci Bull 8:608–610 (in Chinese)

Li BY, Zhang QS, Wang FB (1991) Evolution of the lake in Karakorum-west Kunlun Mountains. Quat Sci 1:64–71 (in Chinese with English abstract)

Li SJ, Zhang HL, Shi YF, Zhu ZY (2008) A high resolution MIS 3 environmental change record derived from lacustrine deposit of Tianshuihai Lake. Quat Sci 28:122–131 (in Chinese with English abstract)

Liu XJ, Lai ZP (2010) Lake level fluctuations in Qinghai Lake in the Qinghai-Tibetan Plateau since the last interglaciation: a brief review and new data. J Earth Environ 1:79–89 (in Chinese with English abstract)

Liu ZC, Wang YJ, Chen Y, Li XS, Li QC (1998) Magnetostratigraphy and sedimentologically derived geochronology of the Quaternary lacustrine deposits of a 3000 m thick sequence in the central Qaidam Basin, Western China. Palaeogeogr Palaeoclimatol Palaeoecol 140:459–473

Liu XJ, Lai ZP, Fan QS, Long H, Sun YJ (2010) Timing for high lake levels of Qinghai Lake in the Qinghai-Tibetan Plateau since the last interglaciation based on quartz OSL dating. Quat Geochron 5:218–222

Liu XJ, Lai ZP, Yu LP, Sun YJ, Madsen D (2012) Luminescence chronology of aeolian deposits from the Qinghai Lake area in the Northeastern Qinghai-Tibetan Plateau and its palaeoenvironmental implications. Quat Geochron 10:37–43

Long H, Lai ZP, Fuchs M, Zhang JR, Yang LH (2012a) Palaeodunes intercalated in loess strata from the western Chinese Loess Plateau: timing and palaeoclimatic implications. Quat Int 263:37–45

Long H, Lai ZP, Fuchs M, Zhang JR, Li Y (2012b) Timing of Late Quaternary palaeolake evolution in Tengger Desert of northern China and its possible forcing mechanisms. Global Planet Change 92–93:119–129

Madsen DB, Ma H, Rhode D, Brantingham PJ, Forman SL (2008) Age constraints on the late Quaternary evolution of Qinghai Lake, Tibetan Plateau. Quat Res 69:316–325

Madsen DB, Lai ZP, Sun YJ, Rhode D, Liu XJ, Brantingham PJ (2013) Late Quaternary Qaidam lake histories and implications for an MIS 3 "Greatest Lakes" period in northwest China. J Paleolimnol. doi:10.1007/s10933-012-9662-x

Mischke S, Lai ZP, Zhang CJ (2013) Re-assessment of the paleoclimate implications of the Shell Bar in the Qaidam Basin, China. J Paleolimnol. doi:10.1007/s10933-012-9674-6

Mischke S, Sun Z, Herzschuh U, Qiao Z, Sun N (2010) An ostracod-inferred large Middle Pleistocene freshwater lake in the presently hyper-arid Qaidam Basin (NW China). Quat Int 218:74–85

Murray AS, Wintle AG (2000) Luminescence dating of quartz using an improved single-aliquot regenerative-dose protocol. Radiat Meas 32:57–73

Murray AS, Wintle AG (2003) The single aliquot regenerative dose protocol: potential for improvements in reliability. Radiat Meas 37:377–381

Ning Y, Liu W, An Z (2009) A 130-ka reconstruction of precipitation on the Chinese Loess Plateau from organic carbon isotopes. Palaeogeogr Palaeoclimatol Palaeoecol 270:59–64

Ou XJ, Lai ZP, Zeng LH, Zhou SZ (2012) OSL dating of glacial sediments from the Qinghai-Tibetan Plateau and its bordering mountains: a review and methodological suggestions. J Earth Environ 3:829–842

Oviatt CG, Madsen DB, Schmitt DN (2003) Late Pleistocene and early Holocene rivers and wetlands in the Bonneville Basin of western North America. Quat Res 60:200–210

Pachur HJ, Wünnemann B, Zhang HC (1995) Lake evolution in the Tengger Desert, Northwestern China, during the last 40000 years. Quat Res 44:171–180

Pigati JS, Quade J, Wilson J, Jull AJT, Lifton NA (2007) Development of low-background vacuum extraction and graphitization systems for ^{14}C dating of old (40–60 ka) samples. Quat Int 166:4–14

Prell WE, Kutzbach JE (1987) Monsoon variability over the past 150,000 years. J Geophys Res 92:8411–8425

Prescott JR, Hutton JT (1994) Cosmic ray contributions to dose rates for luminescence and ESR dating: large depths and long-term time variations. Radiat Meas 23:497–500

Rhode D, Ma HZ, Madsen DB, Brantingham PJ, Forman SL, Olsen JW (2010) Paleoenvironmental and archaeological investigation at Qinghai Lake, western China: geomorphic and chronometric evidence of lake level history. Quat Int 218:29–44

Rhodes TE, Gasse F, Lin RF, Fontes JC, Wei K, Bertrand P, Gibert E, Melieres F, Tucholka P, Wang Z, Chen Z (1996) A Late Pleistocene-Holocene lacustrine record from Lake Manas, Zunggar (northern Xinjiang Western China). Palaeogeogr Palaeoclimatol Palaeoecol 120:105–125

Rick TC, Vellanoweth RL, Erlandson JM (2005) Radiocarbon dating and the "old shell" problem: direct dating of artifacts and cultural chronologies in coastal and other aquatic regions. J Archaeol Sci 32:1641–1648

Roberts HM, Duller GAT (2004) Standardised growth curves for optical dating of sediment using multiple-grain aliquots. Radiat Meas 38:241–252

Shi YF, Liu XD, Li BY, Yao TD (1999) A very strong summer monsoon event during 30–40 ka BP in the Qinghai-Xizang (Tibet) Plateau and its relation to precessional cycle. Chin Sci Bull 44:1851–1858

Shi Y, Yu G, Liu X, Li B, Yao T (2001) Reconstruction of the 30–40 ka BP enhanced Indian monsoon climate based on geological records from the Tibetan Plateau. Palaeogeogr Palaeoclimatol Palaeoecol 160:69–83

Shi XM, Li YL, Yang JC (2008) Climate and tectonic analysis of Manas Lake changes. Scientia Geograph Sin 28:266–271 (in Chinese with English abstract)

Simms AR, DeWitt R, Rodriguez AB, Lambeck K, Anderson JB (2009) Revisiting marine isotope stage 3 and 5a (MIS3–5a) sea levels within the northwestern Gulf of Mexico. Global Planet Change 66:100–111

Sun YJ, Lai ZP, Long H, Liu XJ, Fan QS (2010) Quartz OSL dating of archaeological sites in Xiao Qaidam Lake of the Qinghai–Tibetan Plateau and its implications for palaeoenvironmental changes. Quat Geochronol 5:360–364

Tang LY, Wang SL (1988) The pollen flora in the Gonghe formation of the Gonghe Basin in China. Acta Palaeontol Sin 27:583–608 (in Chinese with English abstract)

Thompson LG, Yao T, Davis ME, Henderson KA, Mosley-Thompson E, Lin P-N, Beer J, Synal H-A, Cole-Dai J, Bolzan JF (1997) Tropical climate instability: the last glacial cycle from a Qinghai-Tibetan ice core. Science 276:1821–1825

Wang FB, Ma CM, Xia XC, Cao QY, Zhu Q (2008) Environmental evolution in Lop Nur since Late Pleistocene and its response to the global changes. Quat Sci 28:150–153 (in Chinese with English abstract)

Webb GE, Price GJ, Nothdurft LD, Deer L, Rintoul L (2007) Cryptic meteoric diagenesis in freshwater bivalves: implications for radiocarbon dating. Geology 37:803–806

Yang X, Scuderi LA (2010) Hydrological and climatic changes in deserts of China since the Late Pleistocene. Quat Res 73:1–9

Yang B, Wang J, Shi Y, Braeuning A (2004) Evidence for a warm-humid climate in arid northwestern China during 40–30 ka BP. Quat Sci Rev 23:537–2548

Yang JF, Lu SW, Zhao H, Cui XF, Lü XH (2006) Lacustrine sediments' U-series age and its significance in the Jiezechaka Lake of Tibet. J Earth Sci Environ 28:6–10 (in Chinese with English abstract)

Yi L, Lai ZP, Yu HJ, Xu XY, Su Q, Yao J, Wang XL, Shi XF (2013) Chronologies of sedimentary changes in the south Bohai Sea, China: constraints from luminescence and radiocarbon dating. Boreas 42:267–284

Yim WW-S, Ivanovich M, Yu K-F (1990) Young age bias of radiocarbon dates in pre-Holocene marine deposits of Hong Kong and implications for Pleistocene stratigraphy. Geo-Marine Lett 10:165–172

Yu LP, Lai ZP (2012) OSL chronology and palaeoclimatic implications of aeolian sediments in the eastern Qaidam Basin of the northeastern Qinghai-Tibetan Plateau. Palaeogeogr Palaeoclimatol Palaeoecol 337–338:120–129

Yu G, Gui F, Shi YF, Zheng YQ (2007) Late marine isotope stage 3 palaeoclimate for East Asia: a data-model comparison. Palaeogeogr Palaeoclimatol Palaeoecol 250:167–183

Yu LP, Lai ZP, Pan T, Han WX OSL chronology and paleoclimatic implications of paleodunes in the mid- and southwestern Qaidam Basin. Sci Cold Arid Regions (in press)

Zhang H, Lei G, Chang F, Fan H, Yang M, Zhang W (2007) Age determination of Shell Bar section in salt lake Qarhan. Qaidam Basin. Quat Sci 27:511–521 (in Chinese with English abstract)

Zhang H, Lei G, Chang F, Pu Y, Fan H, Lei Y, Yang M, Zhang W, Yang L (2008a) Chronology of the Shell Bar section and a discussion on the ages of the Late Pleistocene lacustrine deposits in the paleolake Qarhan, Qaidam basin. Front Earth Sci China 2:225–235

Zhang H, Wang Q, Peng J, Chen G (2008b) Ostracod assemblages and their paleoenvironmental significance from Shell Bar section of palaeolake Qarhan. Qaidam Basin. Quat Sci 28:103–111 (in Chinese with English abstract)

Zhang W, Zhang H, Lei G, Yang L, Niu J, Chang F, Yang M, Fan H (2008c) Elemental geochemistry and paleoenvironment evolution of Shell Bar section at Qarhan in the Qaidam Basin. Quat Sci 28:917–928 (in Chinese with English abstract)

Zhang JR, Lai ZP, Jia YL (2012) Luminescence chronology for late Quaternary lake levels of enclosed Huangqihai lake in East Asian monsoon marginal area in northern China. Quat Geochronol 10:123–128

Zhao XT, Zhang MP, Li DM (2009) Dating of the Sanchahe formation and development of paleolake Kunlun in Golmud city, Qinghai Province. Quat Sci 29:89–97 (in Chinese with English abstract)

Zheng M, Meng Y, Wei L (2000) Evidence of the pan-lake stage in the period of 40–28 k a BP on the Qinghai-Tibet Plateau. Acta Geol Sin 74:266–272

Zhou W, Head MJ, Wang F, Donahue DJ, Jull AJT (1999) The reliability of AMS radiocarbon dating of shells from China. Radiocarbon 41:17–24

Zhu DG, Meng XG, Zhao XT, Shao ZG, Xu ZF, Yang CB, Ma ZB, Wu ZH, Wu ZH, Wang JP (2004) Evolution of an ancient large lake in the southeast of the northern Tibetan Plateau. Acta Geol Sin 78:982–992